Mon. Not. R. Astron. Soc. **000**, 000–000 (1995) Printed 1 February 2008 (MN LATEX style file v1.3)

The soft X-ray properties of a complete sample of radio sources

J. Siebert,[1] W. Brinkmann,[1] R. Morganti,[2,3] C.N. Tadhunter,[4] I.J. Danziger,[5] R.A.E. Fosbury[6,7] and S. di Serego Alighieri[8]

[1] *Max-Planck-Institut für Extraterrestrische Physik, Giessenbachstrasse, D-85740 Garching, Germany*
[2] *Istituto di Radioastronomia, CNR, via Gobetti 101, I-40129 Bologna, Italy*
[3] *Australia Telescope National Facility, CSIRO, PO Box 76, Epping, NSW 2121, Australia*
[4] *Department of Physics, University of Sheffield, Sheffield S3*
[5] *ESO, Karl Schwarzschild Strasse 2, D-85748 Garching, Germany*
[6] *Space Telescope-European Coordinating Facility, Karl Schwarzschild Strasse 2, D-85748 Garching, Germany*
[7] *Affiliated to the Astrophysics Division, Space Science Department, European Space Agency*
[8] *Osservatorio Astrofisico di Arcetri, Largo E. Fermi 5, 50125 Firenze, Italy*

Accepted 1995 November 24. Received 1995 November 9; in original form 1995 March 7

ABSTRACT

We present the soft X-ray (0.1–2.4 keV) properties of a complete sample of 88 southern radio sources derived from the Wall & Peacock 2-Jy sample. It comprises 68 radio galaxies, 18 quasars and 2 BL Lac objects. Whereas both BL Lac objects and all but one quasar are detected in the *ROSAT* All-Sky Survey, the fraction of detected radio galaxies is only ~ 60 per cent. For the undetected sources upper limits to the X-ray flux are given. We confirm the correlation of the soft X-ray luminosity ($L_{\rm x}$) with the core radio luminosity ($L_{\rm r,core}$) for galaxies as well as for quasars using partial correlation analysis, whereas the corresponding correlations between $L_{\rm x}$ and $L_{\rm r,total}$ are probably spurious due to sample selection effects. We also find strong correlations between $L_{\rm x}$ and $L_{\rm r,core}$ for both Fanaroff-Riley type I (FR I) and type II galaxies. The broad-line radio galaxies (BLRGs) and the quasars are at the top end of the X-ray luminosity distribution and the detection rate of these objects generally is higher than that of the narrow- or weak-lined radio galaxies. This indicates the presence of an anisotropic X-ray component in BLRGs and quasars, as predicted by unified schemes for radio sources.

Key words: Galaxies: active Radio sources: general.

1 INTRODUCTION

There is growing evidence that much of the apparent diversity found amongst active galactic nuclei (AGNs) can be explained by anisotropic obscuration and, in the case of radio-loud objects, by relativistic boosting effects resulting from a high-velocity jet. Within this unifying framework, the classification of an AGN is believed to be influenced strongly by the orientation with respect to the line of sight. The subject has been discussed extensively in recent years, for both radio-quiet and radio-loud AGNs (see Antonucci 1993 for a review). Well-defined samples of AGNs with comprehensive observational data on the relevant parameters at different wavelengths are essential for statistically reliable tests of these theories.

In the X-ray waveband, statistical properties of both radio galaxies and quasars have been studied using data obtained mostly with the Imaging Proportional Counter (IPC) on board the *Einstein* satellite. Feigelson & Berg (1983), using a heterogeneous sample of radio galaxies, found a correlation between X-ray luminosity and both total and core radio power. The optical emission lines do not, however, appear to be a good predictor of the X-ray emission. According to these authors, the results can be best explained by assuming that the X-ray emission comes from the hot gas of a putative surrounding cluster. For a sample of forty 3C radio galaxies, Fabbiano et al. (1984) found that FR II galaxies and objects with strong optical emission-line spectra tend to be more powerful in X-rays than those with an FR I morphology and weak or absent optical emission lines. In addition, they confirm a strong correlation between the radio core power and X-ray luminosity. They conclude, in contradiction to Feigelson & Berg (1983), that the X-ray emission in radio galaxies is dominated by the AGN rather than diffuse hot gas.

The key issue at hand, therefore, concerning our un-

derstanding of the X-ray/radio/optical correlations is that of distinguishing between these alternative origins for the X-ray emission.

In the case of quasars, early studies (see e.g., Zamorani et al. 1984; Wilkes & Elvis 1987) showed that two components contribute to the X-ray emission of radio-loud objects. One is isotropic and likely to be present also in radio-quiet quasars. The other appears to be associated with the radio core emission (e.g., by the synchrotron self-Compton mechanism) and is probably beamed. Browne & Murphy (1987) and Kembhavi, Feigelson & Singh (1986) have found strong correlations between the X-ray luminosity and both the extended and the core radio power.

The slope of the correlation between X-ray luminosity and the extended radio power becomes flatter for the less core-dominated radio sources, i.e., for a given extended radio luminosity, the core-dominated sources have significantly stronger X-ray emission. Browne & Murphy (1987) have shown that this behaviour supports the idea of two X-ray components with the beamed one being prominent in the core-dominated quasars. As further confirmation of this, more recent studies of the spectral slope have shown that in radio-loud quasars the soft X-ray spectrum is correlated with the core dominance parameter R: the spectrum gets flatter as R increases (Shastri et al. 1993; Wilkes 1994).

However, none of the studies includes an analysis of a complete sample of both radio galaxies and quasars for which good optical spectroscopic data as well as X-ray and radio observations are available. Recently, a complete sample with such characteristics has been established: it includes 88 southern radio sources and represents a subsample of the Wall & Peacock 2.7-GHz catalogue (Wall & Peacock 1985; Morganti, Killeen & Tadhunter 1993; Tadhunter et al. 1993; di Serego Alighieri et al. 1994). Here we present the soft X-ray properties of these sources using data from both the *ROSAT* All-Sky Survey (Voges 1993) and pointed *ROSAT* observations. Throughout this paper we assume $H_0 = 50$ km s^{-1} Mpc^{-1} and $q_0 = 0$.

2 THE SAMPLE

Our subsample is defined by redshift $z < 0.7$, declination $\delta < 10^{\rm o}$, and it is complete down to a flux density level of 2 Jy at 2.7 GHz. Optical spectra of all sources, including those of the original Wall & Peacock sample with $\delta < 10^{\rm o}$ and no spectroscopic redshift, were taken by Tadhunter et al. (1993) and di Serego Alighieri et al. (1994) with the ESO 3.6-m and 2.2-m telescopes at La Silla, Chile. The redshift constraint was chosen to obtain accurate measurements of the [O III]λ5007 line flux for all objects. In addition, the [O II]λ3727 and Hβ emission-line fluxes were determined to make use of ionization diagnostics. For observational details and the presentation of the results, see Tadhunter et al. (1993) and di Serego Alighieri et al. (1994).

Radio data from the Very Large Array (VLA) and the Australia Telescope Compact Array (ATCA) have been obtained at 5 GHz with an angular resolution of ~ 3 arcsec (Morganti et al. 1993). These data and information from literature (Stickel, Meisenheimer & Kühr 1994; Zirbel & Baum 1995) have allowed a morphological classification of the sources according to the Fanaroff & Riley (1974) convention. In some cases the FR-type could not unambiguously be determined, which is due to either inadequate radio data or the presence of transition sources which show morphological details typical of both FR I and FR II (e.g., PKS 1333−33 or Her A). The adopted classification for this study is given in Table 1. For most of the sources core flux densities are available from literature (see references given in the notes to Table 1).

3 DATA ANALYSIS

3.1 ROSAT All-Sky Survey

We have examined the *ROSAT* All-Sky Survey (RASS) data for the sources in the sample in order to determine their soft X-ray properties or to derive useful upper limit fluxes in the case of non-detections. This has been done using a procedure based on standard commands within the EXSAS environment (Zimmermann et al. 1993). The procedure uses a maximum-likelihood source detection algorithm which returns the likelihood of existence for a X-ray source at the specified radio position, the number of source photons within 5 times the FWHM of the Position Sensitive Proportional Counter (PSPC) point spread function (PSF) and the error in the number of source photons. For the RASS the FWHM of the PSPC point spread function is estimated to be ~ 60 arcsec (Zimmermann et al. 1993)

We consider a radio source to be detected in soft X-rays if the likelihood of existence is greater than 5.91, which corresponds to 3σ. Thus, the statistical probability of identifying a background fluctuation as a source is only 0.27 per cent. In view of the fact that an AGN is known to be present, 3σ is regarded as an appropriate detection criterion. We further note that the probability for a chance coincidence of a X-ray source with a radio source, based on geometrical considerations, is only $\sim 10^{-6}$. If no source is detected at the radio position, the 2σ upper limit on the number of source photons is determined. The RASS exposure of the sources, used to calculate the corresponding count rates, is derived from the vignetting-corrected exposure map and is averaged over the area of the source.

The critical parameter in the calculation of a reliable upper limit is the local X-ray background at the source position. We calculate the local background by selecting a source-free box along the scanning direction of the telescope, but slightly offset from the supposed source position in the Survey. In this way, it is ensured that the background region has an exposure similar to that of the source.

The unabsorbed fluxes are calculated from the count rates by assuming a simple power-law spectrum modified by Galactic absorption, which is parametrized by the neutral hydrogen column density ($N_{\rm H}$) towards the source (Stark et al. 1992) and the photoelectric absorption coefficients of Morrison & McCammon (1983). The photon indices are chosen to be $\Gamma = 1.9$ for galaxies and $\Gamma = 2.15$ for quasars, which represent the class averages of the much larger samples of radio-loud X-ray sources of Brinkmann, Siebert & Boller (1994) and Brinkmann et al. (1995). All luminosities are calculated in the rest frame of the sources, again using the class average power-law indices for the K-correction.

Landscape table to go here.

Table 1.

3.2 Pointed ROSAT observations

In addition to the data from the RASS, 34 sources were in the field of view of pointed *ROSAT* observations. A similar source detection procedure was applied to the data. However, due to the much smaller PSF of the PSPC in pointed observations, the standard extraction radius for source photons is reduced to 2.5 times the FHWM of the PSF for pointed mode at an energy of 0.3 keV. The FWHM depends on the off-axis angle and ranges from ∼40 to ∼65 arcsec for on-axis and for 20 arcmin off-axis observations, respectively. For the sources that appeared extended due to their proximity (see below), the extraction radius was adjusted by hand to ensure the inclusion of all photons from the AGN. For the sources in clusters of galaxies, for which the AGN emission could not be spatially separated from the surrounding cluster emission (0255+05, 0625−53, 0915−11, 1246−41, 1514+07), the standard extraction radius was used as well. This procedure is aimed at constraining the X-ray fluxes to the AGN emission as much as possible. Fluxes and luminosities (see Table 1) are calculated assuming the same spectral parameters as for the RASS data. The errors in the fluxes are determined by photon statistics only and do not include uncertainties in the spectral parameters of the sources. Unless otherwise stated, we use the fluxes from the pointed observations in all further analysis.

3.3 Comparison of the results from the RASS and from pointed observations

3.3.1 X-ray fluxes

Five sources are detected in the pointings that had only upper flux limits from the RASS. Except for PKS 0325+02 (3C 88), the RASS upper limits are well above the flux determined from the pointed observations. For the radio galaxy 3C 88, however, the 95 per cent upper flux limit (0.7×10^{-12} erg cm^{-2} s^{-1}) is almost a factor of 2 lower than the actual flux derived from the pointed observation (1.3×10^{-12} erg cm^{-2} s^{-1}). Given this flux, the source would have been easily detectable in the RASS observation. Obviously, the soft X-ray flux of 3C 88 varied by at least a factor of two between the observations (i.e. within ∼ 12 months).

We compared the soft X-ray fluxes for the 29 sources for which data are available from both the RASS and a pointed observation and found agreement within the errors for most of them. The existing discrepancies can be explained by either variability or the influence of extended X-ray emission. For example, the fluxes of sources associated with clusters (indicated by 'C' in Table 1) tend to be higher in the RASS than in the pointed observations. This is obviously due to the different extraction radii chosen for the two datasets.

Significant differences in the fluxes of the RASS and the corresponding pointed observation also appeared for the quasars PKS 0403−13, 3C 279, PKS 1510−08 and both BL Lac objects. These discrepancies are most likely due to source variability. The source fluxes changed by factors of ∼2 (PKS 0403−13), ∼4 (3C 279) and ∼3.5 (PKS 1510−08) between the two observations. The flux of the BL Lac object PKS 0521−36 decreased by 50 per cent. The most extreme case is PKS 1514−24 (Ap Lib). It is clearly detected in the RASS with a count rate of ∼ 0.063 count s^{-1}, but not in a 3-ks pointed observation. Based on the RASS count rate, ∼ 184 photons are expected in the pointed observation, whereas the 95 per cent upper limit is only ∼ 9 photons. This implies that the source flux decreased by at least a factor of 20 within 3 years.

3.3.2 X-ray extent

Comparing the extent likelihoods of the sources in the RASS and the pointed observations, it turns out that the extent likelihood derived from the RASS observation is not a good predictor of the true source extent unless the value is very high. This is due to the complicated energy and angular dependence of the PSF in the RASS, which can lead to a smearing of otherwise point-like sources, especially for bright objects. 11 sources had a likelihood for source extent greater than 10 in the RASS. Fortunately, 9 of them were also observed in pointed observations and, indeed, three objects turned out to be point-like in X-rays (3C 120, 3C 273, PKS 0620−52). In the case of PKS 0620−52 the RASS value obviously is affected by a second bright X-ray source only 3 arcmin away from the AGN. The remaining two sources, for which no pointed observation is available, either are associated with a known cluster (PKS 2104−25) or have a $B_{\rm gg}$ value (see Section 5.1.2) suggesting a dense environment (PKS 0442−28) and are thus likely to be extended in X-rays as well.

3.4 Previous X-ray observations

There are two sources that were detected with the *Einstein* IPC, but not in the RASS (0034−01, 2356−61). The derived upper limit fluxes from the Survey observation are well above the corresponding IPC fluxes. We converted the 0.5–4.5 keV IPC fluxes to the *ROSAT* energy band by assuming a photon index of 1.9.

For 3C 445, which has previously been claimed to be associated with the strong X-ray source 2A2220−022 (Marshall et al. 1978), we can derive only an upper limit on the flux from the Survey observation. Obviously, 2A2220−022 has been misidentified and it is most likely connected to the cluster A2440, which is located ∼ 50 arcmin north of 3C 445 and within the error box of 2A2220−022. This has already been noted by Pounds (1990), who also reports a marginal detection of 3C 445 in an IPC observation with a flux comparable to our upper limit. Given the uncertainties in the spectral parameters of this source and in the flux conversion from the IPC to *ROSAT*, we use the *ROSAT* upper limit in our analysis. Similarly, 4U1716−01 is most likely not connected to 3C 353, as has been suggested by Forman et al. (1978) and Wood et al. (1984). Again, there is no X-ray source detected at the position of 3C 353 in the RASS, but extended emission is visible to the south-east of 3C 353, at a position which is consistent with the error box of 4U1716−01 and which is probably due to a previously unidentified cluster of galaxies.

4 RESULTS

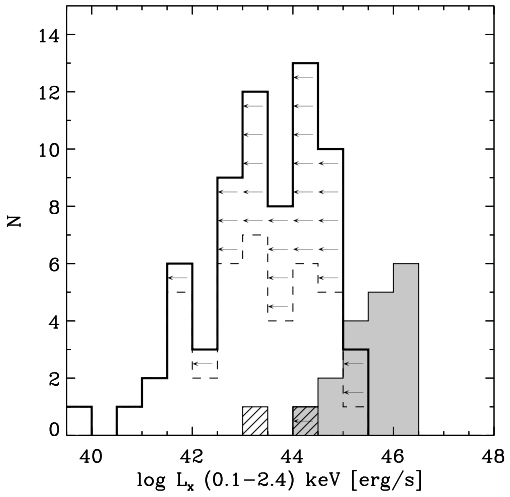

Figure 1. Distribution of X-ray luminosities in the total *ROSAT* energy band (0.1–2.4 keV) for quasars (dark), BL Lacs (hatched) and galaxies (solid line). Upper limits are indicated by arrows.

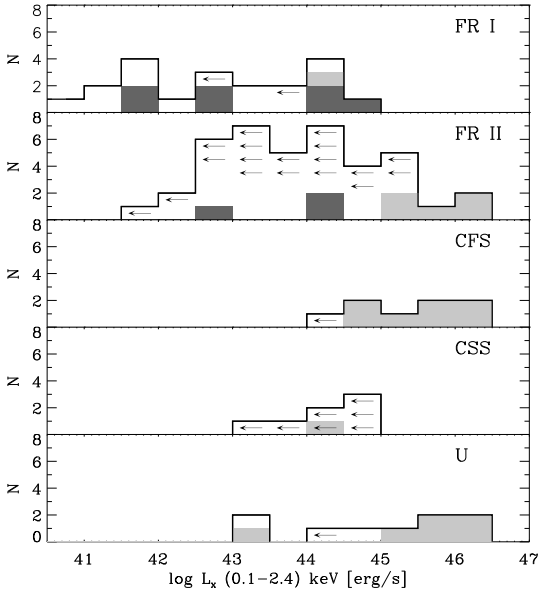

Figure 2. Distribution of the X-ray luminosities for the different radio morphological subgroups. Quasars/BL Lacs and sources associated with clusters are represented by light and dark shading, respectively. Again upper limits are indicated by arrows. The morphological types are described in Table 1.

4.1 Soft X-ray properties

The analysis of the sample resulted in 59 detections and 29 upper limits. Apart from PKS 1151−34, all quasars and BL Lac objects are detected, while for ∼40 per cent of the radio galaxies only upper limits to the X-ray flux could be determined. In Table 1 we present the soft X-ray properties of the objects in our sample together with the relevant information from other wavebands.

In total 16 sources show significantly extended X-ray emission in either the RASS or pointed observations. These sources are marked with 'E' in Table 1. Nine sources appear extended due to the X-ray emission from the associated cluster of galaxies (they are denoted with 'E,C' in Table 1).

The four closest sources in our sample (NGC 253, NGC 1068, Fornax A, Centaurus A) also show extended X-ray emission. NGC 253 is known to have a X-ray halo (Pietsch et al., in preparation), whereas an extended starburst component has been reported for NGC 1068 (Wilson et al. 1992; Ueno et al. 1994). Finally, 3C 270 (Worrall & Birkinshaw 1994) and Hercules A (Leahy 1995) are extended in X-rays as well. The latter object will be discussed in more detail in Section 5.1.2.

In Fig. 1 we show the soft X-ray luminosity distribution for the quasars, BL Lac objects and galaxies in our sample. The galaxies and quasars are well separated with the quasars being brighter in X-rays. Moreover, the galaxies cover a wider range in X-ray luminosity than the quasars. While the quasars are confined to $10^{45} - 10^{46}$ erg s^{-1}, the galaxy luminosities cover five orders of magnitude from 10^{40} erg s^{-1} to 10^{45} erg s^{-1}, with most of the galaxies at the low-luminosity end being of the FR I type.

The distribution of the X-ray luminosities for the radio morphological classes is shown in Fig. 2. At first sight, the FR I type sources seem to be shifted towards lower X-ray luminosities compared with the FR IIs. While there are some very X-ray-luminous FR I galaxies that reach the top end of the FR II distribution, these are either associated with a cluster of galaxies or classified as a BL Lac object. The low-luminosity tail of the FR I distribution overlaps with the region of normal elliptical and spiral galaxies ($L_x = 10^{39} - 10^{42}$ erg s^{-1}, Fabbiano 1989). On the other hand, most of the highly X-ray-luminous FR II type objects are also quasars. We applied ASURV (LaValley, Isobe & Feigelson 1992; Feigelson & Nelson 1985; Isobe, Feigelson & Nelson 1986) to test the hypothesis that the X-ray luminosity distributions for the FR I and FR II type objects are drawn from the same parent population using the narrow-line field radio galaxies only, i.e. excluding galaxies in clusters and broad-line objects (quasars, BLRGs). We find that the luminosity distributions of FR I and FR II type sources are now statistically indistinguishable. This is in contradiction to the results of Fabbiano et al. (1984), who concluded that FR IIs are on average brighter in X-rays than FR Is, although it should be noted that they included broad-line galaxies in their analysis.

The fraction of upper limits among the FR IIs is much higher than among the FR Is. To first order, this is due to a distance effect, because the FR I galaxies are on average at a smaller redshift in this radio flux limited sample, since only the most radio luminous galaxies, i.e. FR IIs, can be seen at higher redshifts. But even considering only those objects that cover the same redshift range ($0.03 \leq z \leq 0.112$, which excludes all low-luminosity FR Is), the detection rate of FR I field radio galaxies (using the RASS results) still tends to be higher (FR I: $4/6 = 67(\pm 33)$ per cent; FR II: $4/15 = 27(\pm 13)$ per cent). Interestingly, the luminosity distributions for the restricted subsamples are now different at the 95 per cent confidence level: compared with the FR IIs, the X-ray luminosites of FR Is are *higher* on average.

The compact flat-spectrum (CFS) and the unclassified (U) sources show the highest X-ray luminosities. In addition, these morphological classes also show very high X-ray

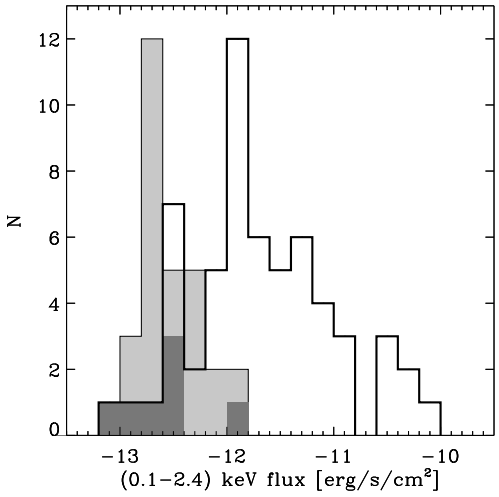

Figure 3. X-ray fluxes of all 88 2-Jy sources in the total 0.1–2.4 keV energy band. Detected sources are plotted with a thick line while sources with upper limits are represented by the light shaded area. Sources that are detected in pointed observations only are indicated by the dark shaded area.

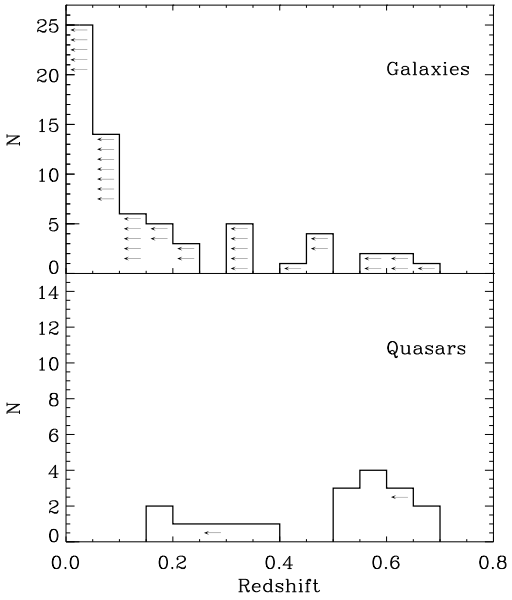

Figure 4. Redshift distributions for galaxies and quasars. Sources that only have an upper limit from the RASS observation are indicated by arrows.

detection rates. Most of the CFS and many U sources are quasars or BL Lac objects, which were just resolved in the radio observations (Morganti et al. 1993), but impossible to classify in terms of radio morphology. Finally, the lack of detections of compact sources with a steep radio spectral index (either compact steep-spectrum (CSS) or GHz-peaked (GPS) sources), already pointed out from the analysis of larger samples (Brinkmann et al. 1994, 1995), is likely to be due to the high redshifts at which these sources are usually found. In fact, there are only two out of 18 radio galaxies detected in the redshift range of the CSS sources (typically $z > 0.2$), and both show broad lines. Nevertheless, it is worth mentioning that the only quasar not detected in soft X-rays is classified as a CSS source as well.

4.2 Undetected sources

In Fig. 3 we plot the flux distribution of all sources in the 0.1–2.4 keV energy band. Apart from the sources that were detected in pointed observations with longer exposure (dark shaded), detections and upper limits are well separated. Nevertheless, the two distributions show an overlap which reflects the inhomogeneous exposure of the sources in the RASS and the variations in the Galactic $N_{\rm H}$ value. The sources detected in pointed observations only are included in the analysis with their RASS upper limit fluxes in this section, because of the generally much longer exposure in pointings compared with the RASS observations.

One possible reason for a non-detection in soft X-rays could be an unusually high value of Galactic absorption along the line of sight. A Kolmogorov-Smirnov test gives a probability of 80 per cent that the $N_{\rm H}$ distributions of detected and undetected sources were drawn from the same parent population. Thus there is no significant bias towards high $N_{\rm H}$ values among the non-detected sources.

The varying exposure of the sources during the RASS does not explain why some sources are detected while others are not. With very few exceptions, the distributions of the exposures for detected and non-detected sources are very similar.

The last possibility, apart from intrinsic source properties, is a distance effect. In Fig. 4 we plot the redshift distributions for galaxies and quasars with upper limits indicated by arrows. In the case of the galaxies it is obvious that the detections and the upper limit sources have markedly different redshift distributions. The majority of the detected sources have redshifts smaller than 0.1 and there are only two galaxies detected beyond $z = 0.25$ (1602+01, 1938−15).

4.3 Correlations

In the following sections we compare the X-ray luminosities of the objects with their emission properties in the radio and the optical wavebands. The correlation and regression analysis including the upper limits was done with ASURV (LaValley et al. 1992).

4.3.1 X-ray – Radio correlations

Figs 5 and 6 show the plots of the 0.1–2.4 keV X-ray luminosity $L_{\rm x}$ versus the total 5-GHz luminosity $L_{\rm r,total}$ and the 5-GHz core luminosity $L_{\rm r,core}$, respectively. The results of the correlation and regression analysis for various object classes are summarized in Table 2, where we also give the respective probabilities that the observed correlations arise by chance. In general, the derived parameters have large uncertainties (all errors are 1σ in Table 2), which is expected given the low number of objects and the large fraction of upper limits. Nevertheless, an inspection of the figures clearly suggests the presence of a correlation between $L_{\rm x}$ and both $L_{\rm r,total}$ and $L_{\rm r,core}$ for quasars as well as for radio galaxies.

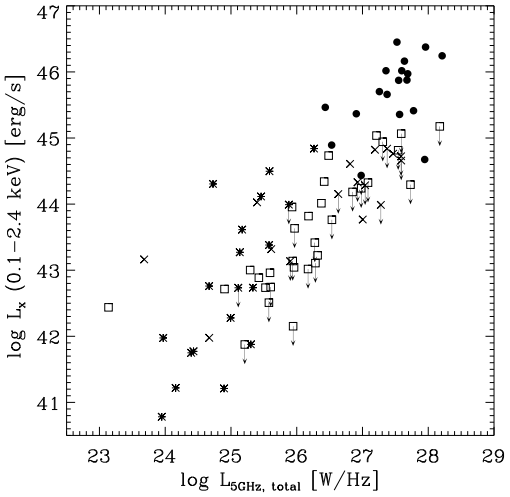

Figure 5. Integrated 0.1-2.4 keV X-ray luminosity versus total 5-GHz radio luminosity (•=quasars, ∗=FR I galaxies, □= FR II galaxies, ×=other galaxies, arrows indicate upper limits).

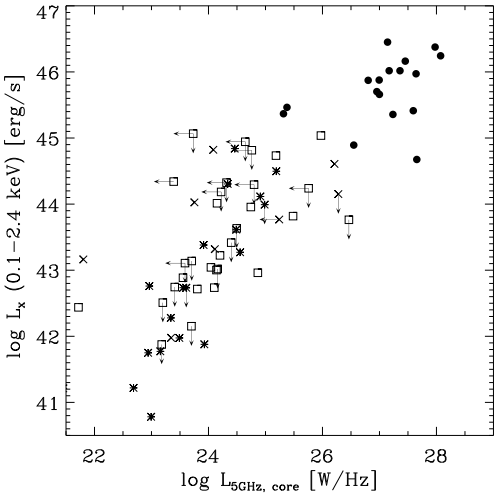

Figure 6. X-ray luminosity versus 5-GHz core luminosity (•=quasars, ∗=FR I galaxies, □= FR II galaxies, ×=other galaxies, arrows indicate upper limits).

This is confirmed by a simple correlation analysis, although, statistically, the correlation probability for quasars is only marginally significant. This is partly due to the low number of objects. Note that the significance of the $L_{\rm x}$ – $L_{\rm r,core}$ correlation is higher than that of the $L_{\rm x}$ – $L_{\rm r,total}$ correlation for both object classes.

In interpreting these correlations one has to consider selection effects, in particular the dependence of the total radio luminosity on redshift z, artificially introduced by the radio flux limit of the original Wall & Peacock sample. $L_{\rm x}$ and $L_{\rm r,core}$ do not depend a priori on redshift, because of the inclusion of upper limit values. Further, the correlations of $L_{\rm x}$ with $L_{\rm r,total}$ and $L_{\rm r,core}$ are not mutually independent since $L_{\rm r,core}$ is also correlated with $L_{\rm r,total}$. Usually, a partial correlation technique is applied to analyse a many-variable problem like this and to disentangle the real correlations from those introduced by the individual dependences amongst the variables. However, these methods fail to account properly for censored data. To deal with these, a new procedure, based on Kendall's τ, was developed to calculate the partial correlation coefficient and to estimate its significance in the presence of upper limits (Akritas & Siebert 1996).

We applied this new procedure to estimate the influence of the $L_{\rm r,total}$ – $L_{\rm r,core}$ and $L_{\rm r,total}$ – z relations on the correlation between $L_{\rm x}$ and both $L_{\rm r,total}$ and $L_{\rm r,core}$. In the case of the quasars, the $L_{\rm x}$ – $L_{\rm r,total}$ correlation seems to be strongly affected by both the redshift bias and the $L_{\rm r,core}$ – $L_{\rm r,total}$ correlation. It turns out that the correlation is no longer statistically significant once both selection effects are properly accounted for. The $L_{\rm x}$ – $L_{\rm r,core}$ correlation is much less affected and the probability of erroneously rejecting the null hypothesis of no correlation is $\lesssim 4$ per cent, which is acceptable given the low number of objects. We thus conclude that there is indeed a correlation between $L_{\rm x}$ and $L_{\rm r,core}$ for quasars and that the $L_{\rm x}$ – $L_{\rm r,total}$ correlation is most likely an artefact of the redshift bias and/or the strong relation between $L_{\rm r,total}$ and $L_{\rm r,core}$ in our sample. The remarkably flat regression slope for quasars in the $L_{\rm x}$ – $L_{\rm r,core}$ correlation is consistent with previous findings. Kembhavi et al. (1986) give 0.465 ± 0.04 as best-fitting slope to a sample of 86 quasars with measured radio core fluxes including X-ray upper limits, and Baker, Hunstead & Brinkmann (1995) report 0.36 ± 0.1 for a large sample of steep-spectrum quasars. However, these results are inconsistent with the findings of Browne & Murphy (1987), who derive a regression slope of 0.75 for a sample of 135 quasars. The difference may be explained by the heterogeneity of their sample and the selection effect they introduce by not including upper limits in their analysis.

The results for the radio galaxies are similar. The $L_{\rm x}$ versus $L_{\rm r,core}$ correlation remains highly significant in the partial correlation analysis, whereas the probability of no correlation between $L_{\rm x}$ and $L_{\rm r,total}$ increases from 0.03 per cent to 7.5 per cent once the effect of redshift is taken into account. Given the much larger sample size compared with the quasars, this result provides evidence for the $L_{\rm x}$ – $L_{\rm r,total}$ correlation being introduced by the redshift bias. Interestingly, the regression parameters for the $L_{\rm x}$ – $L_{\rm r,total}$ and the $L_{\rm x}$ – $L_{\rm r,core}$ correlations are almost identical ($a \sim 0.6 \pm 0.1$). Fabbiano et al. (1984) and Brinkmann et al. (1995) find a slightly steeper regression slope in the case of the galaxies ($\sim 0.8 \pm 0.2$), but consistent within the errors.

We repeated the correlation and regression analysis for the two FR classes separately. Unfortunately, the large number of upper limits among the FR II radio galaxies does not allow a reliable determination of the regression parameters, and the $L_{\rm x}$ – $L_{\rm r,total}$ correlation turns out to be insignificant in the partial correlation analysis. Note that the $L_{\rm x}$ – $L_{\rm r,core}$ correlation remains significant. Formally, we find strong correlations between $L_{\rm x}$ and both $L_{\rm r,core}$ and $L_{\rm r,total}$ for the FR I galaxies. The $L_{\rm x}$ –$L_{\rm r,total}$ correlation, however, is only marginally significant in the partial correlation analysis, whereas the $L_{\rm x}$ – $L_{\rm r,core}$ correlation is obviously not influenced by any of the above-mentioned selection effects, and the regression slope is close to unity. Both findings in-

Table 2. Results of the correlation and regression analysis.

Y	X	Class	N	UL_Y	UL_X	a	b	P	P_{L_c/L_T}	P_z
$\log L_x$	$\log L_{total}$	QSO	18	1	0	0.59±0.26	29.54±7.25	0.081	0.749	0.271
		GAL	68	28	0	0.58±0.10	28.14±2.67	0.0003	0.004	0.075
		FR I	20	2	0	1.37±0.29	8.52±7.28	0.0013	0.067	0.082
		FR II	31	17	0	0.45±0.20	31.30±5.11	0.0053	0.014	0.32
		ALL	88	29	0	0.88±0.08	20.50±2.19	$\ll 10^{-6}$		
$\log L_x$	$\log L_{core}$	QSO	17	0	0	0.30±0.14	37.65±3.79	0.017	0.039	0.017
		GAL	59	20	10	0.63±0.12	27.66±2.85	$< 10^{-6}$	$< 10^{-4}$	$< 10^{-4}$
		FR I	20	2	0	1.00±0.18	19.08±4.40	0.0002	0.007	0.014
		FR II	30	16	8	0.58±0.26	28.94±6.28	0.0011	0.012	0.016
		ALL	78	20	10	0.77±0.06	24.40±1.48	$\ll 10^{-6}$		
$\log L_x$	$\log L_{opt}$	QSO	18	1	0	0.84±0.16	19.54±4.87	0.0006		0.0017
$\log L_x$	$\log L_{[O\ III]}$	QSO	18	1	0	0.92±0.20	5.65±8.58	0.0021		0.007
		FR II	30	16	0	0.41±0.12	25.97±4.93	0.19		
		QSO & FR II	48	17	0	0.92±0.11	4.86±4.54	$\ll 10^{-6}$		0.005
		FR I	19	2	12	0.67±0.30	16.61±11.78	0.025		0.069

X and Y denote the independent and the dependent variables, respectively. N is the total number of objects while UL_X and UL_Y are the number of upper limits in the independent and the dependent variables. Linear regression has been performed assuming $\log Y = a \log X + b$. All errors are 1σ. P is the probability that no correlation is present, whereas P_{L_c/L_T} and P_z denote the same probability but with the effects of the $L_{r,core}$ – $L_{r,total}$ correlation and redshift excluded, respectively.

dicate a contribution to the X-ray emission from the active nucleus in FR I galaxies.

4.3.2 X-ray – optical correlations

In Fig. 7 we plot the soft X-ray luminosity versus the optical luminosity. The rest-frame optical luminosity was calculated from the V magnitudes, using the formula of Allen (1976) for flux conversion. We applied an energy power-law index of $\alpha = 0.5$ for the K-correction. There is an excellent correlation between the optical and the X-ray luminosities for quasars, which is not affected by the redshift bias. The best-fitting regression slope is 0.84 ± 0.16. The correlation found is slightly steeper than the value obtained from the much larger *ROSAT*/Condon quasar sample (Brinkmann et al. 1995, 0.75 ± 0.12), but is still within the mutual errors. Boyle et al. (1993) derive a slope of 0.88 ± 0.08 from an analysis of the optical and the soft X-ray luminosity functions of an X-ray-selected sample of quasars. Avni & Tananbaum (1986) give 0.8 as the best-fitting regression slope for a sample of 94 *Einstein*-detected quasars and 60 upper limits, whereas Wilkes et al. (1994) find a slightly flatter slope (0.71) for an even larger sample, but still in agreement with our results. No correlation between the optical and the X-ray luminosities is observed for the radio galaxies.

In Fig. 8 we plot the soft X-ray luminosity versus the [O III]λ5007 line luminosity. There is a highly significant correlation visible for the quasars and the regression slope is consistent with unity. Partial correlation analysis shows that this result is not spurious due to the possible correlations of L_x and $L_{O\,III}$ with $L_{r,total}$, $L_{r,core}$ or z. Therefore L_x seems to be physically related to $L_{O\,III}$, which argues for the narrow-line gas being photionized by the AGN. Although we fail to find a significant correlation for the FR II radio galaxies as well, we note a smooth transistion from

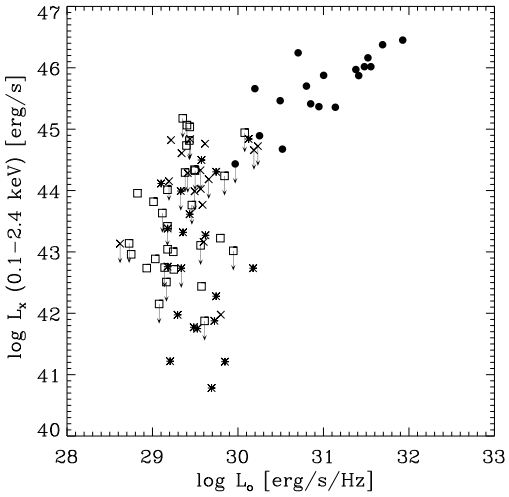

Figure 7. Optical luminosity versus soft X-ray luminosity (•=quasars, ∗=FR I galaxies, □= FR II galaxies, ×=other galaxies, arrows indicate upper limits).

quasars to FR IIs, whereas FR I galaxies definitely show different behaviour with, in general, much lower [O III] luminosity compared with their X-ray emission.

5 DISCUSSION

Two main points are apparent from the above analysis. First, there is a very large range in X-ray luminosity over which the radio galaxies can be observed. This is probably the effect of different mechanisms at work in producing the X-rays. Secondly, anisotropic X-ray emission from the ac-

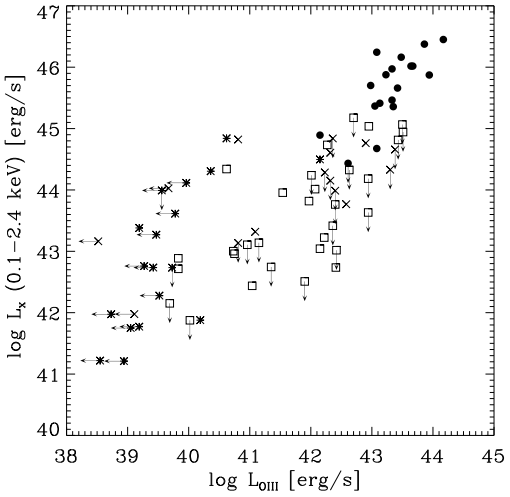

Figure 8. [O III] line luminosity versus X-ray luminosity (∗= FR I, □= FR II, ×=other galaxies, •= quasars, arrows indicate upper limits).

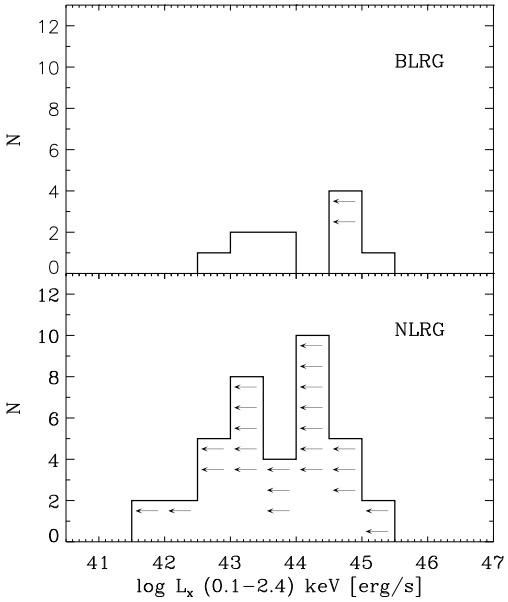

Figure 9. X-ray luminosity distribution for broad-line and narrow- or weak-lined radio galaxies.

tive nucleus is likely to be present also in radio galaxies as indicated by the correlation of X-ray luminosity with radio core power in FR I galaxies. In the next sections we discuss the role of the emission from the active nucleus in different object classes, the implications for unified schemes and possible mechanisms responsible for the X-ray emission in radio galaxies.

5.1 Sources of X-ray emission from radio galaxies

5.1.1 The contribution of the AGN

The correlation of $L_{\rm x}$ with $L_{\rm r,core}$ for both quasars and radio galaxies suggests that the X-ray emission is related to the radio emission from the core of the AGN, for example by synchrotron self-Compton or inverse Compton processes in the radio jet. The flat slope of the $L_{\rm x}$ – $L_{\rm r,core}$ correlation for quasars might be due to unresolved radio emission in the cores of the quasars, which is not related to the X-ray emission. This is plausible given the high redshift of the objects and has already been pointed out by Kembhavi et al. (1986). Indeed, they find a steepening of the regression slope as they pass from quasars with resolved cores to unresolved radio sources with flat or inverted spectra, which presumably are dominated by 'real' core emission.

A subset of radio galaxies in our sample shows broad emission lines (Tadhunter et al. 1993; Shaw et al. 1995). In Fig. 9 we plot the distribution of X-ray luminosities for galaxies classified as broad-line (BLRG, upper panel) and the ones with narrow or weak lines (lower panel). We excluded the FR I galaxies because none of the BLRGs is unambiguously classified as FR I. The histogram shows the higher detection rate and, on average, higher X-ray luminosity of the BLRGs compared with the other radio galaxies. A statistical test with ASURV reveals that the two distributions are different at the 99.5 per cent confidence level.

This result is consistent with the unified scheme for high-power radio sources (Barthel 1989). In this scheme, it is proposed that we see the nucleus directly in the case of quasars, whereas in the narrow-line radio galaxies (NLRGs) the nucleus is 'hidden' by a combination of relativistic beaming effects and dust/gas obscuration. BLRGs are supposed to be observed at intermediate angles. Since the obscuration is likely to be significant at soft X-ray energies, we would expect a higher X-ray detection rate amongst the quasars and BLRGs, because they are less obscured. Further evidence that the BLRGs are intermediate objects can be derived from the fact that the optical spectra of BLRGs do show differences compared with those of quasars, including redder continua and steeper Balmer decrements (e.g., Osterbrock, Koski & Phillips 1976). This can be interpreted in terms of partial obscuration. Finally, Turner & Pounds (1989) conclude from an *EXOSAT* study of emission-line AGNs that intrinsic absorption is quite common in BLRGs, which again argues for BLRGs being intermediate objects. On the other hand, although most of our BLRGs do show red continua, some of them may also be nearby quasars where the host galaxy can be seen. This would also explain the observed deficiency of nearby quasars in our sample: there are 24 FR II radio galaxies with a redshift $z \leq 0.2$ in our sample. Assuming that all FR IIs are 'misdirected' quasars and, further, that FR IIs with angles to the line of sight below 45° are classified as quasars, we would expect to see 7±2.7 quasars with $z \leq 0.2$, whereas 3 are observed. The discrepancy, although marginal, increases if one takes into account that our sample may be biased towards core-dominated sources due to the relatively high radio selection frequency.

Although evidence for anisotropic nuclear X-ray radiation in radio galaxies is mainly restricted to the broad-line sources, such radiation could contribute to the narrow- or weak-lined radio galaxies as well. Monte Carlo simulations (Morganti et al. 1995) have shown that the observed differences in the radio core detection rates of FR I and FR II radio galaxies (Morganti et al. 1993) can be explained if the jets of FR I galaxies are characterized by on average lower Lorentz factors compared with FR II galaxies. If there is also

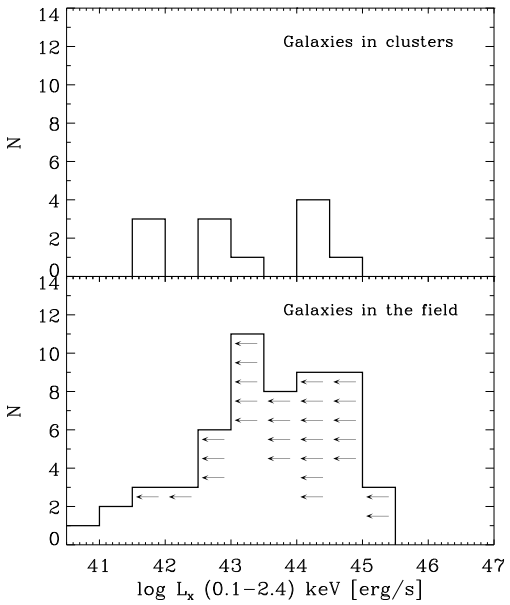

Figure 10. X-ray luminosity distributions for radio galaxies in the field and those associated with a cluster.

an anisotropic contribution to the X-ray emission in these galaxies, which is affected by the same Lorentz factors as the radio emission, we expect a higher X-ray detection rate for the FR I galaxies, since the radiation is then emitted in a broader beam and is thus more likely to be observed.

In Section 4.1 we have presented indications for a higher detection rate and higher X-ray luminosities of FR I type galaxies compared with FR IIs, in carefully chosen subsamples to avoid various selection effects. Unfortunately, the significance of the results is limited by the small number of objects and, although we restricted the analysis to a small range in redshift, there is still a tendency for FR II galaxies to be at higher redshifts. Nevertheless, the model of an anisotropic and less beamed X-ray component in FR I galaxies compared with FR II represents a viable explanation of our data, but the statistical evidence is not particularly strong. Larger samples of FR I and FR II galaxies are required to decide if the soft X-ray detection rate and luminosities of FR I galaxies are really higher.

We note, however, that evidence for non-thermal X-ray emission from low-power radio galaxies has recently been reported by Worrall & Birkinshaw (1994). After deconvolving the extended and unresolved X-ray emission components, they find a correlation with slope unity between the unresolved X-ray luminosity and the 5-GHz core luminosity. This can be readily explained if the X-rays originate from the inner regions of a parsec-scale radio jet (Worrall & Birkinshaw 1994).

5.1.2 ISM

Thermal bremsstrahlung from a hot interstellar medium is known to be an important component of the X-ray emission from galaxies (e.g. Canizares 1987). This emission may come from diffuse gas distributed on very different spatial scales: clusters, small groups or galactic haloes. With *ROSAT* it has become feasible to prove the presence of extended thermal emission even in isolated and/or distant radio galaxies. Recently, evidence for an extended emission component has been reported for several distant radio galaxies (e.g. Worrall et al. 1994; Crawford & Fabian 1995). However, apart from the sources already mentioned in Section 4.1, no evidence for extended emission has been found in our sample, but, as already pointed out in Section 3.3.2, the information on the X-ray size of the sources is not conclusive in the RASS.

Various models have been proposed to explain the correlations of $L_{\rm x}$ with $L_{\rm r,total}$ and $L_{\rm r,core}$ for radio galaxies in the context of a thermal origin of the X-ray emission. For example, Feigelson & Berg (1983) relate the correlation of $L_{\rm r,total}$ with $L_{\rm x}$ in a sample of powerful (mostly FR II) 3CR galaxies to the presence of hot X-ray emitting gas in the putative cluster environment of these objects, which confines the radio lobes and thus also increases the radio emission due to inhibited adiabatic expansion losses. Fabbiano, Gioia & Trinchieri (1989) suggested that the hot ISM in radio galaxies fuels the AGN via accreting cooling flows and thus the strength of the radio core emission is related to the amount of gas (and hence X-ray emission) in those objects. The strong correlations found for FR I radio galaxies in our sample could support these arguments, since nearby FR Is are frequently found in cluster environments (e.g. Prestage & Peacock 1988). We note, however, that the correlations also hold for the apparently isolated nearby FR I objects and that the $L_{\rm x}$ – $L_{\rm r,total}$ correlation may be an artefact of the redshift bias (see Section 4.3.1)

In order to investigate further the possible contribution of thermal emission from a hot intracluster medium, we plot in Fig. 10 the distribution of the X-ray luminosities for the radio galaxies in clusters (upper panel) and for field galaxies (lower panel). The X-ray detection rate of the cluster sources is much higher than that of the field glaxies, which is most likely explained by the on average lower redshifts of the cluster sources compared with the field galaxies. We derive a (marginally significant) ~ 85 per cent probability that the luminosity distributions of the two subsamples are different, with the cluster sources showing slightly higher X-ray luminosity. In order to quantify better the contribution of the cluster medium to the X-ray emission, we have collected the values of the so-called $B_{\rm gg}$ parameter, which is a measure of the distribution of galaxies around a given source (Lilly & Prestage 1987; Prestage & Peacock 1988; Yates, Miller & Peacock 1989). There does not appear to be any correlation between the $B_{\rm gg}$ parameter and the X-ray luminosity. However, a possible positive correlation may be masked by the fact that the source detection algorithm systematically misses parts of the extended X-ray flux for sources with high values of $B_{\rm gg}$. We therefore conclude that the cluster X-ray emission, despite our efforts to isolate the AGN, still may contribute to the X-ray flux in some objects, but that the cluster emission is on average not the *dominant* source of X-ray emission in our sample of radio galaxies.

A group of radio galaxies in the sample showing high X-ray luminosities ($L_{\rm x} \gtrsim 10^{43}$ erg s^{-1}) appear to be isolated objects without strong emission lines in the optical spectrum. The most extreme case is certainly Hercules A.*

* Whether or not Her A is associated with a cluster of galaxies has not yet been unambiguously decided. Contradictory results,

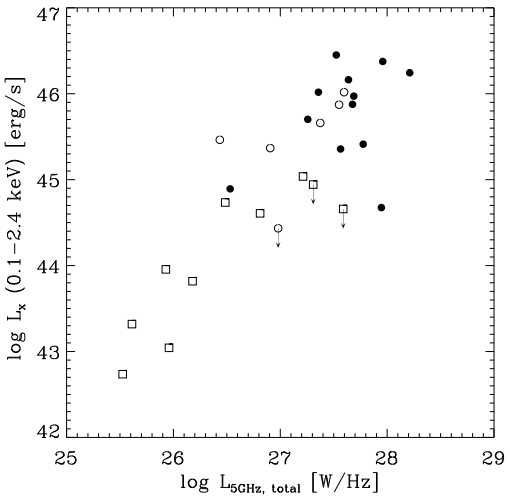

Figure 11. Soft X-ray luminosity versus radio luminosity for BLRGs (squares) and quasars (circles). Flat -spectrum objects with $\alpha_{2.7}^{4.8} \leq 0.5$ are plotted with filled symbols.

Other similar objects are 0305+03, 0325+02, 1637−77 and 1954−55.

Ponman et al. (1994) have recently reported the discovery of a so-called fossil group, a single elliptical galaxy that is considered to be the result of the merging process of a compact group. This merging is believed not to affect the X-ray halo of the group (Ponman & Bertram 1993) and the ellipticals formed in this way will have a high X-ray luminosity though they appear isolated. The typical X-ray luminosities of these groups are $L_{\rm x} = 10^{41} - 4 \times 10^{43}$ erg s^{-1} (Ponman & Bertram 1993; Ebeling, Voges & Böhringer 1994). These luminosities are low compared with the X-ray luminosity observed for Her A, both by *ROSAT* ($L_{\rm x} = 6 \times 10^{44}$ erg s^{-1}) and by *Einstein* ($L_{0.5-4.5{\rm keV}} = 1.4 \times 10^{44}$ erg s^{-1}, Feigelson & Berg 1983). However, good agreement between Her A and the objects studied by Ponman et al. (1994) seems to be present with respect to some other source characteristics, like the extension of the X-ray emission and the effective radius ($R_{\rm e}$) of the optical galaxy. Furthermore, evidence for a recent or ongoing merger has been reported from optical observations (Sadun & Hayes 1993). Perhaps additional X-ray emission associated with the active nucleus has to be considered in the case of Her A, given the high radio power of this galaxy.

The process suggested by Ponman et al. (1994) can be important in understanding the X-ray emission from isolated objects although spatial information is necessary to test the hypothesis for other radio sources.

Finally, the low-power tail of the distribution of the FR I galaxies ($L_{\rm x} = 10^{41} - 10^{42}$ erg s^{-1}, see Fig. 2) is consistent with the X-ray emission from normal early-type galaxies as found by Forman, Jones & Tucker (1985), and in fact there are two objects, Cen A and For A, that are included in both samples. Forman et al. (1985) find typical X-ray luminosities ranging from $L_{\rm x} \sim 10^{39}$ to $\sim 8 \times 10^{41}$ erg s^{-1} and a frequent occurrence of hot coronae. The dominant X-ray emission in these cases has been interpreted as thermal emission from hot gas which has been accumulated as a result of mass loss from evolved stars.

based on galaxy counts or spatial correlation functions, have been reported in the literature (e.g. Yates et al. 1989; Allington-Smith et al. 1993).

5.2 X-rays and the nature of the radio-optical correlations

It has been known for some time that the optical emission-line luminosity is closely correlated with the radio power for radio galaxies (e.g. Hine & Longair 1979; Rawlings & Saunders 1991). It is generally assumed that this correlation arises because the strength of the EUV/X-ray continuum responsible for photoionizing the warm gas clouds increases with radio power. If this AGN photoionization model holds, we would expect to observe a general increase in the strength of the AGN X-ray emission with radio power.

The problem we face in testing the X-ray photoionization model is that part of the X-ray emission from the galaxies in our sample is likely to be due to thermal ISM emission (see above). We therefore concentrate on the broad-line objects (BLRGs and quasars) for which we are confident that most of the X-ray emission is emitted by the AGN. Fig. 11 shows a plot of X-ray luminosity against radio power for the combined sample of BLRGs and quasars. There is a general increase in the X-ray luminosity moving from BLRGs to quasars, and the level of this increase is just as expected on the basis of the photoionization models and the radio-optical correlations. Indeed, there is almost a direct proportionality between the X-ray and the emission-line luminosities (see Fig. 8 and Table 2). The results are generally consistent with the idea that the nuclei of BLRGs are the illuminating AGNs in the lower power/lower redshift objects, while quasars are the illuminating AGNs in the higher power/higher redshift objects.

One possible complication is that the flat-spectrum objects in our sample may be dominated by the relativistically beamed core component, which may not have a large influence on the ionization of the gas because of the narrowness of the beam. However, we see from Fig. 11 that the flat- and steep-spectrum sources follow approximately the same distributions in the diagram, so the beamed component does not appear to affect the result.

6 CONCLUSIONS

We have presented an analysis of the soft X-ray properties of a complete sample of 88 radio sources (68 galaxies, 18 quasars and 2 BL Lac objects) derived from the Wall & Peacock (1985) sample. The X-ray data, taken from the *ROSAT* All-Sky Survey, the *ROSAT* public data archive, and previous *Einstein* measurements, finally resulted in 59 detections and 29 upper limits. While all but one quasar is detected, ~ 40 per cent of the galaxies only have upper limits to the X-ray flux from the Survey. The detection rate of the galaxies is clearly redshift dependent.

We find strong correlations between $L_{\rm x}$ and $L_{\rm r,core}$ for all object classes, which can be interpreted in terms of a significant contribution of the AGN to the X-ray luminosity. A partial correlation analysis shows that the correlation of

$L_{\rm x}$ with $L_{\rm r,total}$ is probably an artefact of the redshift dependence of both luminosities and/or the strong correlation of $L_{\rm r,total}$ with $L_{\rm r,core}$. Furthermore, there are correlations present between $L_{\rm x}$ and the optical continuum as well as with [O III]-line luminosity for quasars.

The high detection rate of BLRGs and quasars, as well as the observed correlation between X-ray and both the radio core and the [O III] luminosities suggests that the X-ray emission of these objects is dominated by the contribution of the AGN. This is consistent with orientation-dependent unification schemes for powerful radio sources. Excluding the BLRGs and the quasars, the case for an AGN component of the X-ray emission is less clear, although the strong correlation between $L_{\rm x}$ and $L_{\rm r,core}$ in FR I radio galaxies argues for a nuclear contribution to the X-ray emission.

The X-ray emission of the narrow- or weak-lined radio galaxies is more likely dominated by the contribution of the host galaxies, groups or clusters. The X-ray luminosity of some FR I galaxies is consistent with the emission from the ISM of normal ellipticals, whereas for the high-luminosity objects additional mechanisms are required. There are some isolated galaxies with a relatively high X-ray luminosity ($L_{\rm x} > 10^{43}$ erg s^{-1}), which show no strong optical emission lines. These objects could be single elliptical galaxies resulting from the merging process of a compact group, as suggested by Ponman et al. (1994).

ACKNOWLEDGMENTS

The *ROSAT* project is supported by the Bundesministerium für Bildung, Wissenschaft, Forschung and Technologie (BMBF) and by the Max-Planck Society. JS and WB thank their colleagues from the *ROSAT* group for their support. This research has made use of the NASA/IPAC Extragalactic Data Base (NED) which is operated by the Jet Propulsion Laboratory, California Institute of Technology, under contract with the National Aeronautics and Space Administration.

REFERENCES

Akritas M.G., Siebert J., 1996, MNRAS, in press
Allen C.W., 1976, Astrophysical Quantities. The Athlone Press, London
Allen S.W., Fabian A.C., 1994, MNRAS, 269, 409
Allington-Smith J.R., Ellis R.S., Zirbel E.L., Oemler A., 1993, ApJ, 404, 521
Antonucci R., 1993, ARA&A, 31, 473
Avni Y., Tananbaum H., 1986, ApJ, 305, 83
Baker J.C., Hunstead R.W., Brinkmann W., 1995, MNRAS, 277, 553
Barthel P.D., 1989, ApJ, 336, 319
Boyle B.J., Griffiths R.E., Shanks T., Stewart G.C., Georgantopoulos I., 1993, MNRAS, 260, 49
Brinkmann W., Siebert J., Boller T., 1994, A&A, 285, 812
Brinkmann W., Siebert J., Reich W., Fürst E., Reich P., Voges W., Trümper J., Wielebinski R., 1995, A&AS, 109, 147
Browne I.W.A., Murphy D.W., 1987, MNRAS, 226, 601
Canizares C.R., 1987, in Kormendy J., Knapp G.R, eds, Proc. IAU Symp. 117, Dark Matter in the Universe. Reidel, Dordrecht, p.165
Crawford C.S., Fabian A.C., 1995, MNRAS, 273, 827
Davis D.S., Mushotzky R.F., Mulchaey J.S., Worrall D.M., Birkinshaw M., Burstein D., 1995, ApJ, 444, 582
di Serego Alighieri S., Danziger I.J., Morganti R., Tadhunter C.N., 1994, MNRAS, 269, 998
Duncan R.A., White G.L., Wark R., Reynolds J.E., Jauncey D.L., Norris R.P., Taaffe L., Savage A., 1993, Proc. Astron. Soc. Aust., 10, 310
Ebeling H., Voges W., Böhringer H., 1994, ApJ, 436, 44
Fabbiano G., 1989, ARA&A, 27, 87
Fabbiano G., Miller L., Trinchieri G., Longair M., Elvis M., 1984, ApJ, 277, 115
Fabbiano G., Gioia I.M., Trinchieri G., 1989, ApJ, 347, 127
Fanaroff B.L., Riley J.M., 1974, MNRAS, 167, 31P
Feigelson E.D., Berg C.J., 1983, ApJ, 269, 400
Feigelson E.D., Nelson P.I., 1985, ApJ, 293, 192
Feigelson E.D., Laurent-Muehleisen S.A., Kollgaard R.I., 1995, ApJ, 449, L149
Forman W., Jones C., Cominsky L., Julien P., Murray S., Peters G., Tananbaum H., Giaconni R., 1978, ApJS, 38, 357
Forman W., Jones C., Tucker W., 1985, ApJ, 293, 102
Hine R.G., Longair M.S., 1979, MNRAS, 188, 111
Isobe T., Feigelson E.D., Nelson P.I., 1986, ApJ, 306, 490
Jackson N., Browne I.W.A., Warwick R.S., 1993, A&A, 274, 79
Kembhavi A., Feigelson E.D., Singh K.P., 1986, MNRAS, 220, 51
LaValley M., Isobe T., Feigelson E.D., 1992, BAAS, 24, 839
Leahy D., 1995, UK *ROSAT* Newsletter 7, 10
Lilly S.J., Prestage R.M., 1987, MNRAS, 225, 531
Marshall F.E., Mushotzky R.F., Boldt E.A., Holt S.S., Rothschild R.E., Serlemitsos P.J., 1978, Nat, 275, 624
Morganti R., Killeen N.E.B., Tadhunter C.N., 1993, MNRAS, 263, 1023
Morganti R., Oosterloo T.A., Fosbury R.A.E., Tadhunter C.N., 1995, MNRAS, 274, 393
Morrison R., McCammon D., 1983, ApJ, 270, 119
Osterbrock D.E., Koski A.T., Phillips M.M., 1976, ApJ, 206, 898
Ponman T.J., Bertram D., 1993, Nat. 363, 51
Ponman T.J., Allan D.J., Jones L.R., Merrifield M., McHardy I.M., Lehto H.J., Luppino G.A., 1994, Nat, 369, 462
Pounds K.A., 1990, MNRAS 242, 20p
Prestage R.M., Peacock J.A., 1988, MNRAS, 230, 131
Rawlings S., Saunders R., 1991, Nat, 349, 138
Sadun A.C., Hayes J.J.E., 1993, PASP, 105, 379
Shastri P., Wilkes B.J., Elvis M., McDowell J., 1993, ApJ, 410, 29
Shaw M., Tadhunter C., Dickson R., Morganti R., 1995, MNRAS, 275, 703
Slee O.B., Sadler E.M., Reynolds J.E., Ekers R.D., 1994, MNRAS, 269, 928
Stark A.A., Gammie C.F., Wilson R.W., Bally J., Linke R.A., Heiles C., Hurwitz M., 1992, ApJS, 79, 77
Staubert R., 1992, in Brinkmann W., Trümper J., eds, X-ray emission from active galactic nuclei and the cosmic X-ray background. MPE Report 235, 42
Stickel M., Meisenheimer K., Kühr H., 1994, A&AS, 105, 211
Tadhunter C.N., Morganti R., di Serego Alighieri S., Fosbury R.A.E., Danziger I.J., 1993, MNRAS, 263, 999
Turner T.J., Pounds K.A., 1989, MNRAS, 240, 833
Ueno S., Mushotzky R.F., Koyama K., Iwasawa K., Awaki H., Hayashi, I., 1994, PASJ, 46, L71
Voges W., 1993, Adv. Space Res., 13 (12), 391
Wall J.V., Peacock J.A., 1985, MNRAS, 216, 173
Wilkes B.J., 1994, in Bicknell G.V., Dopita M.A., Quinn P.J. eds, ASP Conf. Ser. Vol. 54, The 1st Stromlo Symposium, The Physics of Active Galaxies. Astron. Soc. Pac., San Francisco, p.41
Wilkes B.J., Elvis M., 1987, ApJ, 323, 243
Wilkes B.J., Tananbaum H., Worrall D.M., Avni Y., Oey M.S., Flanagan J., 1994, ApJS, 92, 53

Wilson A.S., Elvis M., Lawrence A., Bland-Hawthorn J., 1992, ApJ, 391, L75
Wood K.S., Meekins J.F., Yentis D.J., et al., 1984, ApJS, 56, 507
Worrall D.M., Birkinshaw M., 1994, ApJ, 427, 134
Worrall D.M., Lawrence C.R., Pearson T.J., Readhead A.C.S., 1994, ApJ, 420, L17
Yates M., Miller L., Peacock J.A., 1989, MNRAS, 240, 129
Zamorani G. Maccacaro T., Giommi P., Tananbaum H., 1984, ApJ, 278, 28
Zimmermann H.U., Belloni T., Izzo C., Kahabka P., Schwentker O., 1993, MPE Report 244
Zirbel E.L., Baum S.A., 1995, ApJ, 448, 548

Table 1. Soft X-ray properties of the 2-Jy sample and relevant information from other wavebands.

(1)	(2)	(3)	m_V (4)	z (5)	t (6)	log N_H (7)	f_x (8)	S/P (9)	L_x (10)	L_c (11)	L_t (12)	(13)	B_{gg} (14)	Co
0023−26	G	OB-238	19.50	0.322	323	20.27	< 0.17	S	<43.99		27.28	CSS	21	
0034−01	G	3C 15	18.00	0.073	510	20.51	0.37 ± 0.10	E	42.96	24.87	25.59	II	67	
0035−02	G	3C 17	19.00	0.220	566	20.45	1.61 ± 0.28	S	44.61	26.21	26.81	II?	85	BI
0038+09	G	3C 18	18.50	0.188	352	20.74	3.03 ± 0.54	S	44.73	25.18	26.49	II	33	BI
0039−44	G		19.50	0.346	274	20.43	< 0.31	S	<44.33		26.93	U		
0043−42	G		17.00	0.116	321	20.31	< 0.20	S	<43.11	<23.59	26.28	II	17	
0045−25	G	NGC 253	8.04	0.001	346	20.11	1.78 ± 0.20	S/P	39.88	20.75	22.03	CH		E
0055−01	G	3C 29	14.56	0.045	286	20.49	0.08 ± 0.01	P	41.88	23.93	25.30	I	102	C
0105−16	G	3C 32	20.00	0.400	398	20.22	< 0.22	S	<44.33	<24.32	27.08	II		
0117−15	G	3C 38	21.00	0.565	281	20.28	< 0.30	S	<44.82	<24.76	27.54	II		
0123−01	G	3C 40	13.16	0.018	438	20.55	0.42 ± 0.02	S/P	41.77	23.16	24.43	I	101	E,
0131−36	G	NGC 612	13.90	0.030	384	20.27	< 0.19	S	<41.88	23.18	25.21	II	47	
0159−11	QSO	3C 57	16.38	0.669	329	20.29	2.81 ± 0.42	S	46.02	27.17	27.60	II		
0213−13	G	3C 62	18.50	0.147	387	20.28	< 0.25	S	<43.42	24.40	26.28	II		
0235−19	G	OD-159	21.30	0.620	361	20.42	< 0.43	S	<45.07	<23.73	27.59	II		
0240−00	G	NGC 1068	9.61	0.004	250	20.55	39.66 ± 2.14	S/P	42.44	21.72	23.14	II		E
0252−71	G		19.00	0.566	344	20.55	< 0.24	S	<44.73		27.59	CSS		
0255+05	G	3C 75	14.40	0.023	267	20.97	2.48 ± 0.32	S/P	42.76	22.96	24.67	I	225	E,
0305+03	G	3C 78	13.84	0.029	440	20.86	5.02 ± 0.65	S	43.27	24.56	25.13	I	42	
0320−37	G	Fornax A	9.42	0.005	249	20.38	1.51 ± 0.05	S/P	41.21	21.45	24.90	I		E
0325+02	G	3C 88	14.85	0.030	469	20.94	1.31 ± 0.17	P	42.72	23.80	24.90	II	51	
0347+05	G		19.90	0.339	350	21.13	< 0.30	S	<44.29	<24.80	27.73	II		
0349−27	G	OE-283	16.80	0.066	481	20.00	< 0.28	S	<42.75	23.41	25.60	II	33	
0403−13	QSO	OF-105	17.17	0.571	370	20.55	3.04 ± 0.27	S/P	45.88	27.00	27.68	CFS		
0404+03	G	3C 105	18.50	0.089	327	21.08	< 0.37	S	<43.14	23.71	25.94	II	106	
0405−12	QSO	OF-109	14.82	0.574	365	20.59	11.25 ± 0.24	S/P	46.45	27.14	27.52	II		
0409−75	G		21.70	0.693	733	20.97	< 0.42	S	<45.18		28.18	II		
0428−53	G		13.00	0.038	255	19.90	0.84 ± 0.12	S/P	42.74	23.56	25.33	I	440	E,
0430+05	G	3C 120	14.20	0.033	545	21.03	65.14 ± 8.49	S/P	44.50	25.19	25.59	I	-29	BI
0442−28	G	OF-271	18.50	0.147	197	20.35	0.97 ± 0.39	S	44.01	24.15	26.38	II	280	E
0453−20	G	OF-289	13.99	0.035	431	20.41	0.35 ± 0.17	S	42.28	23.34	25.00	I	164	
0518−45	G	Pictor A	16.20	0.035	524	20.65	16.63 ± 1.45	S/P	43.96	24.74	25.93	II	49	BI
0521−36	BLL		14.50	0.055	599	20.52	15.52 ± 1.18	S/P	44.33	25.28	26.10	I	38	
0620−52	G		15.50	0.051	1037	20.71	3.51 ± 0.33	S/P	43.61	24.49	25.17	I		
0625−53	G		15.38	0.054	1185	20.73	8.07 ± 0.90	S/P	44.03	23.75	25.40	II?		E,
0625−35	G	OH-342	16.50	0.055	685	20.85	9.54 ± 1.07	S	44.12	24.91	25.46	I		C
0637−75	QSO		15.75	0.651	646	20.98	6.89 ± 1.20	S/P	46.38	27.98	27.96	CFS		
0736+01	QSO	OI 61	16.47	0.191	338	20.93	4.04 ± 0.62	S/P	44.89	26.55	26.53	CFS		
0806−10	G	3C 195	18.00	0.110	235	20.89	< 0.75	S	<43.63	24.50	25.97	II		

Table 1 – *continued*

(1)	(2)	(3)	m_V (4)	z (5)	t (6)	log N_H (7)	f_x (8)	S/P (9)	L_x (10)	L_c (11)	L_t (12)	(13)	B_{gg} (14)	Co
0842−75	QSO		18.90	0.524	420	20.97	2.28 ± 0.56	S	45.66	27.00	27.37	CJ		
0859−25	G	OJ-299	18.50	0.305	467	20.96	< 0.34	S	<44.24	<25.76	26.98	II		
0915−11	G	Hydra A	13.90	0.054	412	20.69	52.56 ± 4.64	S/P	44.84	24.46	26.26	I	160	E,
0945+07	G	3C 227	17.30	0.086	437	20.48	0.32 ± 0.02	S/P	43.04	24.04	25.96	II	14	Bl
1136−13	QSO	OM-161	16.08	0.554	351	20.56	3.25 ± 0.52	S	45.87	26.80	27.55	II		
1151−34	QSO	OM-386	17.84	0.258	142	20.89	< 0.72	S	<44.43		26.98	CSS		
1216+06	G	3C 270	11.41	0.006	432	20.21	1.06 ± 0.03	S/P	41.22	22.69	24.16	I		E
1226+02	QSO	3C 273	12.86	0.158	371	20.25	113.80 ± 1.95	S/P	46.16	27.45	27.64	CJ		
1246−41	G	NGC 4696	11.39	0.009	341	20.92	41.40 ± 5.27	S/P	43.16	21.81	23.68	U		E,
1251−12	G	3C 278	12.69	0.015	306	20.55	0.57 ± 0.13	S	41.75	22.94	24.40	I	103	
1253−05	QSO	3C 279	17.75	0.538	296	20.35	8.20 ± 0.31	S/P	46.24	28.07	28.21	U		
1306−09	G	OP-10	20.50	0.464	289	20.47	< 0.51	S	<44.84		27.37	CSS		
1318−43	G	NGC 5090	12.57	0.011	293	20.93	1.80 ± 0.62	S	41.98	23.49	23.97	I		
1322−42	G	Cen A	7.84	0.002	291	20.92	3.51 ± 0.42	S/P	40.78	22.99	23.95	I		E
1333−33	G	IC 4296	11.61	0.013	306	20.61	1.29 ± 0.10	S/P	41.98	23.34	24.67	I/II		C
1355−41	QSO		15.86	0.313	328	20.73	3.97 ± 0.70	S	45.37	25.32	26.91	II		
1510−08	QSO	OR-017	16.52	0.361	147	20.91	6.15 ± 0.93	S/P	45.70	26.95	27.26	U		
1514+07	G	3C 317	13.96	0.035	450	20.46	37.13 ± 1.67	S/P	44.31	24.34	24.73	I	143	E,
1514−24	BLL	Ap Librae	15.08	0.048	371	20.94	1.69 ± 0.50	S/P	43.25	25.17	25.29	CJ		
1547−79	G		19.00	0.483	116	20.99	< 0.59	S	<44.94	<24.65	27.31	II		Bl
1549−79	G		18.50	0.150	116	20.98	< 1.29	S	<44.15	26.28	26.63	CFS		
1559+02	G	3C 327	15.88	0.104	497	20.81	< 0.20	S	<43.02	24.16	26.17	II		
1602+01	G	3C 327.1	20.50	0.462	495	20.80	0.81 ± 0.33	S	45.04	25.97	27.21	II	-178	Bl
1637−77	G		15.50	0.041	157	20.95	1.34 ± 0.63	S	43.00	24.14	25.29	II		
1648+05	G	Her A	18.50	0.154	515	20.80	5.68 ± 1.80	S/P	44.82	24.09	27.19	I/II	46	E
1717−00	G	3C 353	15.36	0.031	161	20.51	< 0.33	S	<42.15	23.70	25.95	II		
1733−56	G		18.00	0.098	160	20.92	1.46 ± 0.65	S	43.82	25.48	26.18	II		Bl
1814−63	G		18.00	0.063	125	20.89	< 0.76	S	<43.14		25.90	CSS		
1839−48	G		17.50	0.112	108	20.75	< 1.65	S	<43.99	24.99	25.88	I		
1932−46	G		18.50	0.231	296	20.65	0.21 ± 0.02	P	43.77	<25.24	27.00	II?		
1934−63	G		18.40	0.183	86	20.79	< 1.14	S	<44.29		27.04	CSS	67	
1938−15	G	OV-164	20.00	0.452	349	20.98	0.46 ± 0.24	S	44.76		27.47	U		
1949+02	G	3C 403	16.50	0.059	435	21.21	< 0.20	S	<42.51	23.20	25.58	II		
1954−55	G		16.50	0.060	212	20.67	1.47 ± 0.50	S	43.38	23.91	25.58	I		
1954−38	QSO		17.07	0.630	304	20.81	0.72 ± 0.36	S	45.36	27.24	27.56	CFS		
2058−28	G	OW-297.8	15.16	0.038	453	20.84	< 0.84	S	<42.73	23.61	25.11	I	118	C
2104−25	G	OX-208	15.80	0.037	426	20.74	1.27 ± 0.36	S	42.89	23.55	25.42	II	155	E,
2128−12	QSO	OX-148	15.46	0.501	360	20.66	5.81 ± 0.71	S	46.02	27.36	27.36	CFS		
2135−14	QSO	OX-158	15.91	0.200	354	20.68	13.59 ± 1.52	S/P	45.46	25.38	26.43	II		
2135−20	G	OX-258	19.40	0.635	366	20.53	< 0.16	S	<44.66		27.59	CSS		Bl

Table 1 – *continued*

(1)	(2)	(3)	m_V (4)	z (5)	t (6)	log N_H (7)	f_x (8)	S/P (9)	L_x (10)	L_c (11)	L_t (12)	(13)	B_{gg} (14)	Comm (15
2152−69	G		14.30	0.027	319	20.41	6.49 ± 0.23	S/P	43.32	24.11	25.61	I/II		BLRG
2203−18	QSO	OY-106	18.50	0.618	312	20.42	0.16 ± 0.02	P	44.68	27.66	27.95	CFS		
2211−17	G	3C 444	17.80	0.153	312	20.42	1.90 ± 0.42	S/P	44.34	<23.39	26.42	II	105	E,C
2221−02	G	3C 445	17.00	0.057	235	20.70	0.37 ± 0.04	P	42.74	24.10	25.53	II	-5	BLRG
2243−12	QSO	OY-172.6	16.45	0.630	146	20.68	2.95 ± 0.85	S	45.97	27.64	27.69	CFS		
2250−41	G		19.00	0.310	241	20.15	< 0.28	S	<44.18	<24.22	26.85	II		
2314+03	G	3C 459	18.70	0.220	370	20.72	< 0.23	S	<43.76	26.46	26.54	II		
2345−16	QSO	OZ-176	17.50	0.576	302	20.31	1.02 ± 0.28	S	45.41	27.59	27.78	U		
2356−61	G		16.00	0.096	177	20.38	0.39 ± 0.10	E	43.22	24.20	26.32	II		

Columns (1) – (5) Source identification and optical properties taken from NED. Column (6) Exposure (in seconds) in the ROSAT All-Sky S
(7) Logarithm of the Galactic N_H value (Stark et al. 1992) used for the conversion from countrate to flux. Column (8) Unabsorbed 0.1-2
units of 10^{-12} erg s^{-1} cm^{-2}. Where available, the fluxes from the pointed observations are given. Column (9) S = Survey, P= pointed ob
Einstein observation. Column (10) Log of 0.1–2.4 keV luminosity. Columns (11),(12) Log of core and total 5-GHz radio luminosities in W
are from Morganti et al. (1993), Duncan et al. (1993), Slee et al. (1994) or Morganti et al. (in preparation). Column (13) Adopted radio mo
Morganti et al. (1993), Stickel et al. (1994) or Zirbel & Baum (1995). I = FR I, II = FR II, CSS = compact steep-spectrum, CFS = compact
CH = core/halo, CJ = core/jet, U = unclassified. Column (14) B_{gg} clustering parameter, taken from Prestage & Peacock (1988), Lilly & P
and Yates et al. (1989). Column (15): BLRG = broad-line radio galaxy, E = source significantly extended in X-rays or flux determinati
surrounding diffuse emission, C = associated with known cluster of galaxies. Column (16) References to publications of pointed ROSAT
(A94) Allen & Fabian 1994; (C95) Crawford & Fabian 1995; (D95) Davis et al. 1995; (F95) Feigelson, Laurent-Muehleisen & Kollgaard 1995;
Browne & Warwick 1993; (L95) Leahy 1995; (S92) Staubert 1992; (W92) Wilson et al. 1992; (Wo94) Worrall & Birkinshaw 1994.